# Li-O2 Battery Discharge Redox Mediation by Triarylmethyl Cations

**Erik Askins**
University of Illinois at Chicago
**Marija Zoric**
SLAC National Accelerator Laboratory, Stanford University https://orcid.org/0000-0001-7296-0121
**Rachid Amine**
Argonne National Laboratory
**Khalil Amine**
Chemical Science and Engineering Division, Argonne National Laboratory https://orcid.org/0000-0001-9206-3719
**Ksenija Glusac** ( glusac@uic.edu )
University of Illinois at Chicago https://orcid.org/0000-0002-2734-057X

**Article**

**Keywords:** Li-O2, electrochemistry, electrocatalysis, batteries, redox mediator

**Posted Date:** April 20th, 2022

**DOI:** https://doi.org/10.21203/rs.3.rs-1519289/v1

**Li-$O_2$ Battery Discharge Redox Mediation by Triarylmethyl Cations**

*Erik J. Askins,[1,2] Marija R. Zoric[3], Rachid Amine[4], Khalil Amine[2,5,6] and Ksenija D. Glusac[1,2]*

*[1]Department of Chemistry, University of Illinois at Chicago, Chicago, Illinois, USA*
*[2]Chemical Sciences and Engineering Division, Argonne National Laboratory, Lemont, Illinois, USA*
*[3]Stanford PULSE Institute, SLAC National Accelerator Laboratory, Menlo Park, CA, USA*
*[4]Material Science Division, Argonne National Laboratory, Lemont, Illinois, USA*
*[5]Department of Material Science and Engineering, Stanford University, Stanford, CA, USA*
*[6]Institute for Research and Medical Consultants (IRMC), Imam Abdulrahman Bin Faisal University (IAU), Al Safa, Dammam, Saudi Arabia*

Corresponding author: glusac@uic.edu
Subjects: Li-$O_2$, electrochemistry, electrocatalysis, batteries, redox mediator

**Abstract**
Low discharge capacities resulting from electronically insulating $Li_2O_2$ film growth on carbon electrodes is a major impediment to Li-$O_2$ battery commercialization. Redox mediation is an effective strategy to drive oxygen chemistry into solution, avoiding surface-mediated $Li_2O_2$ film growth and extending discharge lifetimes. However, to continue improving upon prior research, exploration of new classes of redox mediators and discovery of novel selection criteria is required. Herein, we report a new class of triarylmethyl cations which are effective at enhancing discharge capacities up to 26-fold. Surprisingly, we observe that redox mediators with more positive redox mediator reduction potentials, and thus more sluggish kinetics for reaction with oxygen, lead to larger discharge capacities because of their improved ability to suppress the surface-mediated reduction pathway. This result provides important structure-property relationships for future improvements in redox-mediated $O_2$/$Li_2O_2$ discharge capacities. To aid future redox mediator discovery, we applied a chronopotentiometry model to investigate the zones of redox mediator standard reduction potentials and concentrations needed to achieve efficient redox mediation at a given current density. This analysis is expected to guide future redox mediator exploration.

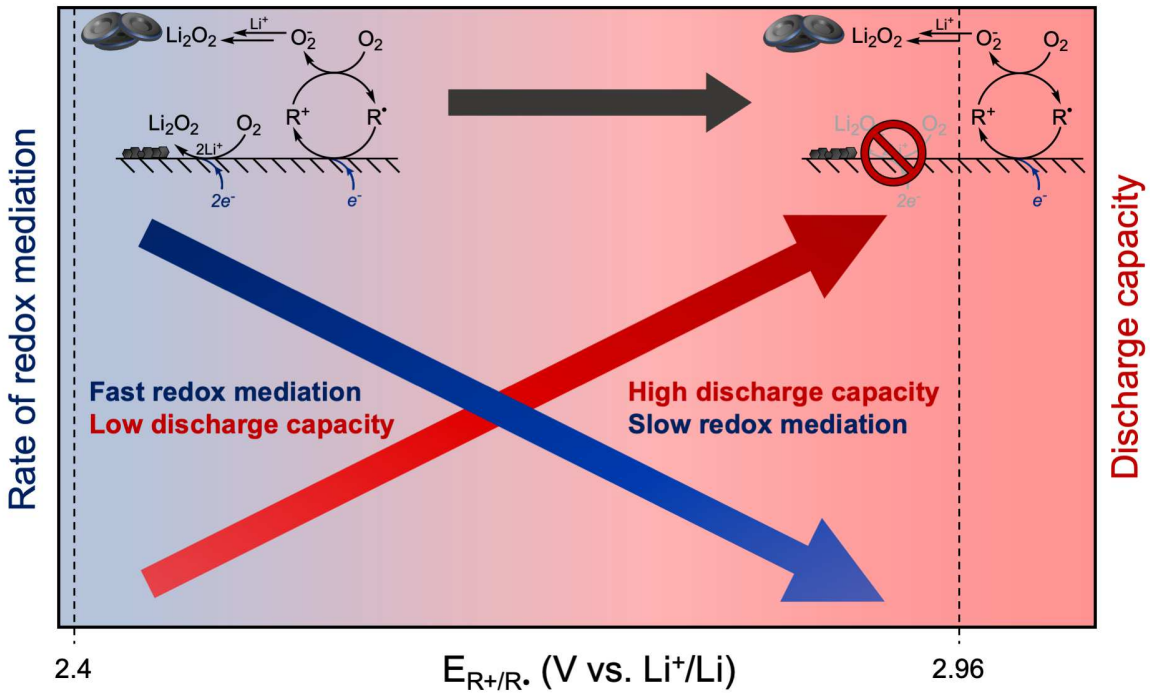


**Introduction**

The Li-oxygen battery exhibits tremendously high theoretical specific energy and is receiving intense interest as a next generation energy system for replacement of the ubiquitous Li-ion battery, which is widely believed to be approaching its performance plateau. In a typical Li-$O_2$ cell, $Li_2O_2$ is formed through an initial $Li^+$-coupled electron transfer step to form an unstable $LiO_2$ intermediate. The $LiO_2$ intermediate undergoes either a second $Li^+$-coupled electron transfer or disproportionation reaction to ultimately yield $Li_2O_2$.[1,2] Though the Li-$O_2$ battery promises large energy density and capacities, the extent to which it can deliver on this promise is contingent upon the mechanisms by which solid $Li_2O_2$ growth is mediated. After its initial reduction at the carbon cathode, subsequent reduction or disproportionation steps proceed in two different locations: in one case, the $LiO_2$ intermediate may stay on the electrode surface and be further reduced to $Li_2O_2$, generating a thin layer of $Li_2O_2$ which electronically passivates the electrode, resulting in premature cell death[1,3]. Alternatively, the reduced oxygen species may dissolve into the electrolyte and, through disproportionation, generate $Li_2O_2$ away from the electrode, delivering large battery capacities. With normal Li-$O_2$ electrolytes (additive-free, non-polar organic solvents), solubility of reduced oxygen intermediates is low, and the electrode-mediated process dominates. Therefore, it is paramount to control the oxygen reduction reaction (ORR) pathway and drive it into solution. Select polar additives, like $H_2O$ and $NO_3^-$[4,5], and solvents, like DMSO[6], have demonstrated themselves able to move the discharge into solution by increasing the solubility of $Li^+$ and $LiO_2$ and delivering increased discharge capacities. However, some of these additives have detrimental effects on the long-term cell cycle life[7], thus there is a need for exploration of additional methods.

To boost the solution-based mechanism of $Li_2O_2$ formation, a series of redox-active compounds were tested as electrolyte additives in Li-oxygen batteries[6–22]. While the overall role of these additives is to shift the $Li_2O_2$ formation site from the electrode surface deeper into the solution phase, their mechanism of action varies to include either an outer-sphere redox mediation or an inner-sphere catalysis. For example, quinone-based additives catalyze the $Li_2O_2$ formation in solution via the inner-sphere mechanism involving an oxygen-quinone intermediate that is formed in a reaction between reduced quinone and molecular oxygen[8,9,12,17–19,21]. This catalytic quinone performance improves as the standard reduction potential of the quinone/quinone radical anion couple is tuned more positive than the $O_2/LiO_2$ potential ($E(O_2/LiO_2)$=2.65 V vs $Li^+/Li$), effectively lowering the overpotential for peroxide formation[9]. Such shift in the quinone reduction potential can be achieved either via the introduction of electron-withdrawing groups into the quinone framework[9] or via addition of water that solvates and stabilizes the reduced quinone anion[8]. Li-$O_2$ batteries with quinone-based additives have been shown to form large disk-like, toroidal $Li_2O_2$ particles on carbon electrodes, a hallmark morphology of the solution-phase mechanism[25]. The discharge capacities of quinone-containing batteries are up to 100-fold improved relative to a non-quinone containing standard[18]. An example of redox mediation was demonstrated with viologen-type derivatives, where the electrolyte additive serves simply as an outer-sphere electron delivery vehicle to facilitate the superoxide formation away from the electrode surface[13,14]. More recently, an interesting new class of non-redox active catalysts were also explored, based on the biomimetic catalytic disproportionation of superoxide into $O_2$ and peroxide[15,16].

Once discharged, recharging the battery and regenerating $O_2$ and Li presents itself as another performance-limiting hurdle for Li-$O_2$ batteries. Firstly, large overpotentials, typically larger than 1 V, are required to oxidize insulating $Li_2O_2$ deposits and only those which reside on the carbon electrode will be affected by the charging process. At such large oxidizing potentials, cell components, like the solvent and carbon electrode, are susceptible to degradation. Redox mediation is again an effective strategy to address these concerns. Here, redox mediation proceeds through oxidation of the mediator at the electrode at lower overpotentials than those where undesired side reactions occur. Oxidized mediators then deliver an electron hole needed to oxidize $Li_2O_2$. Several inorganic anions have been introduced as charging redox mediators ($I^-$, $Br^-$ and $NO_3^-$)[26–28]. However, inability to tune oxidation potentials through synthetic design and negative effects on battery efficiency, resulting from altered discharge products and corrosive side reactions, have led researchers to explore organic compounds for charging redox mediation[26,27,29]. Many compounds and functional groups have been investigated and shown success in reducing the charging overpotential[11,20,24,30–40], but the majority of them have shown poor long-term stability and performance loss after many discharge-charge cycles[41,42]. The π-system containing cores of many redox mediators have a propensity to react with in situ generated $^1O_2$, leading to deactivation[42–45]. Owing to their lack of a π-system, the nitroxyl-based, e.g. (2,2,6,6-tetramethylpiperidin-1-yl)oxyl (TEMPO), molecules emerged as the most promising candidates with the best stability. Indeed, when joint 2,5-di-tert-butyl-1,4-benzoquinone (DBBQ)/TEMPO discharge/charge redox mediators are employed, long-term stability has been achieved, demonstrating that joint redox mediators are a viable way towards a highly efficient and recyclable Li-$O_2$ battery[46].

Despite excellent progress made with redox mediators, their lack of chemical diversity has prevented further developments in the field. For example, most of the discharge mediators are quinone-based and the large number of compounds from this family, with electron withdrawing and donating groups, have already been explored. Following our group's interest in redox-active organic compounds as catalysts and co-catalysts in electrochemistry[43–53], we investigate here a new type of discharge mediator for Li-$O_2$ batteries, based on triarylmethyl cation motifs (Scheme 1a). Computational screening at the density functional theory (DFT) level was used to evaluate the thermodynamic parameters that control the inner-sphere and outer-sphere catalysis mechanisms for the $O_2$/$Li_2O_2$ reduction by the triarylmethyl cations under study. Follow-up cyclic voltammetry (CV) evaluation revealed significant catalytic activity for a selection of outer-sphere redox mediators with the fastest rates of reaction between mediator and oxygen resulting from redox mediator with more negative reduction potentials ($E_{R+/R\bullet}$). When tested for their effect on Li-$O_2$ discharge capacity, capacity enhancements up to 26-fold were seen, which is competitive with the best reported quinone-based mediators. Interestingly, battery discharge capacities were not found to scale with catalytic rates. Instead, discharge capacities increased for the mediators with sluggish catalytic rates (more positive $E_{R+/R\bullet}$) because of their ability to maintain more positive cell potentials and effectively suppress the baseline, surface-mediated reduction of oxygen. Complementary chronopotentiometry modeling revealed that ORR redox mediation can still be achieved for mediators with reduction potentials significantly more positive than what has been explored, but they must be utilized at high concentrations to compensate for the loss of thermodynamic driving force for reaction between redox mediator and oxygen. This work introduces a new family of highly active redox mediators and reveals important criteria for designing future redox mediators which should be operated at more positive potentials and high concentrations for further improvement to Li-$O_2$ battery discharge lifetimes.

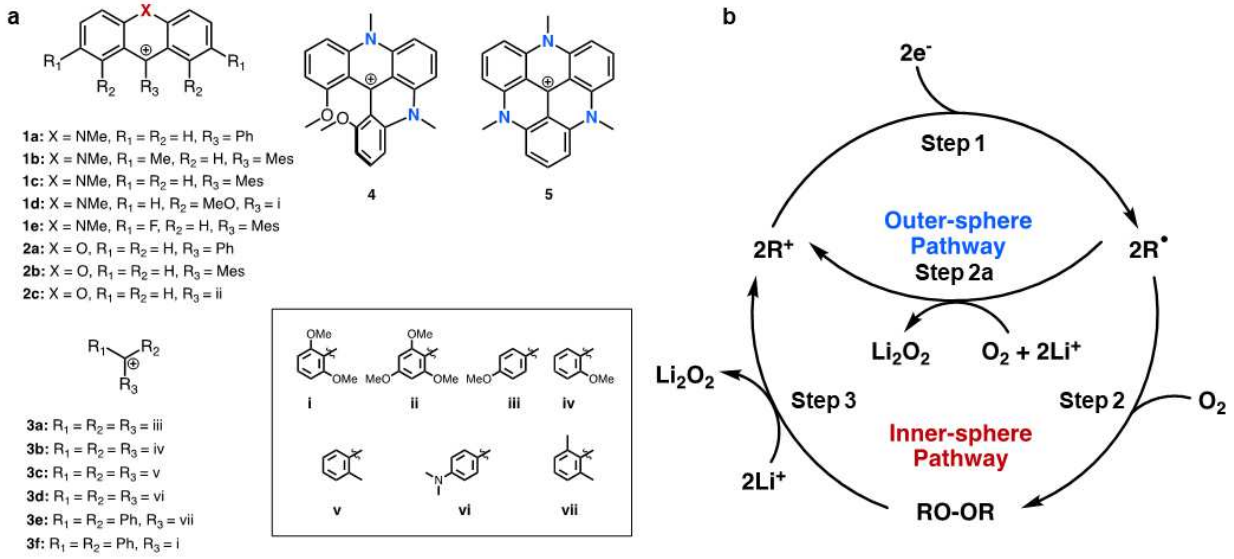

**Figure 1.** a) Structures of triarylmethyl cations from the triphenylmethyl, acridinium and xanthylium families. b) Mechanistic overview of the inner-sphere (peroxide formation) and outer-sphere (redox mediation) pathways.

## Results and Discussion

**Model compounds.** Triarylmethyl cations investigated here consist of acridinium (compounds **1a-e**, **4** and **5**), xanthylium (compounds **2a-c**) and triphenylmethyl (compounds **3a-f**) frameworks, as shown in Figure 1a (synthesis of these compounds is described in the Methods section). Structural diversity in the investigated cations was brought about by introduction of heteroatoms, like N or O, directly into the conjugated motifs and substitution on aryl rings with electron-withdrawing (fluorine) and donating (methyl, methoxy and amine) groups. Two plausible oxygen reduction catalysis mechanisms were explored, namely an outer- or inner-sphere pathway, as shown in Figure 1b. Both mechanisms are initiated by the one-electron reduction of triarylmethyl cation to form a neutral radical $R^{\bullet}$, so the catalytic overpotential is directly related to the standard reduction potential $E^0(R^+/R^{\bullet})$. Our cations appear ideal for this type of reactivity because their $E^0(R^+/R^{\bullet})$ values are situated at a similar position to the $O_2/Li_2O_2$ couple (2.96 V vs. $Li^+/Li$)[51,57–62]. Furthermore, modification of reduction potentials to suit the redox mediation application can be accomplished with relative ease through structural changes like the introduction of electron-donating and withdrawing groups, which shift $E^0(R^+/R^{\bullet})$ to more negative and positive potentials, respectively[51,59,63]. For efficient redox mediation, $R^{\bullet}$ must be stable and persistent in the electrolyte solution. While organic radicals often react parasitically via radical-radical dimerization[64–66], our neutral radicals are expected to be stable because of radical spin delocalization across extended conjugated cores. Moreover, the presence of sterically bulky phenyl substituents is expected to prevent radical-radical dimerization[67]. In the outer-sphere pathway, $R^{\bullet}$ reduces $O_2$ via electron transfer that regenerates the cationic species $R^+$, while the inner-sphere mechanism involves the reaction of $R^{\bullet}$ with $O_2$ to form the peroxide RO-OR (Figure 1b). Some of the radicals $R^{\bullet}$ in Figure 1a have been shown previously to react rapidly with $O_2$ to form RO-OR[58,68], which prompted us to investigate this mechanistic pathway. The catalytic cycle closure in the inner-sphere pathway is achieved by the formation of $Li_2O_2$ through reaction of RO-OR with $Li^+$-cations.

**Computational screening.** Thermodynamic evaluations of the inner- and outer-sphere mechanism were performed at the DFT level of theory by calculating the $\Delta G^0$ values for the formation of $R^{\bullet}$ ($\Delta G^0_1$, Step 1, Scheme 1), reaction between $R^{\bullet}$ and $O_2$ ($\Delta G^0_2$, Step 2) and reaction between RO-OR and $Li^+$-cations ($\Delta G^0_2$, Step 3). Full computational details can be found in the Section 2 of the SI. The calculated standard $R^+/R^{\bullet}$ potentials and $\Delta G^0$ values were used to construct a flowchart which predicts the activity of proposed cations as inner- or outer-sphere redox mediators (Scheme S1, SI). For example, Step 1 filters out candidates with computed reduction potentials outside an established window for oxygen catalysis based on the following arguments: the $E^0(R^+/R^{\bullet})$ value must be more negative than the standard reduction potential for $O_2/Li_2O_2$ (2.96 V vs. $Li^+/Li$)[69], to ensure that the subsequent inner and outer-sphere steps are thermodynamically downhill. Furthermore, the molecular catalyst must be reduced at potentials that are more positive than the reduction of $O_2$ at the electrode (the standard

reduction potential for $O_2/O_2^-$ couple is 2.4 V vs. $Li^+/Li$)[70], to ensure that redox mediation efficiently competes with the non-catalyzed process. These important values have been marked out in the potential scale shown in Figure 2a, along with computed $E^0(R^+/R^\bullet)$ values. The catalysts with $E^0(R^+/R^\bullet)$ values that are more positive than $E^0(O_2/Li_2O_2)$ and more negative than $E^0(O_2/O_2^-)$ were eliminated from further analysis (to account for inaccuracy of the DFT method, a +/- 0.30 V error allowance was introduced to set the upper and lower limits to be 3.26 and 2.10 V vs. $Li^+/Li$).

$E^0(R^+/R^\bullet)$ values were calculated according to computational methods described previously[71], and the values matched reasonably well with experimentally observed potentials for selected cations measured by cyclic voltammetry (CV) (Table S6, SI). The variation in reduction potentials is largely as expected: highly electron-withdrawing oxygen heteroatom make xanthylium-based cations significantly easier to reduce and they appear on the more positive end of the potential scale. Conversely, acridinium-based cations, which feature a more weakly electron-withdrawing heteroatom (nitrogen) appear at more negative potentials. Furthermore, within a family of cations (e.g. 1, 2 or 3), introducing electron-withdrawing (e.g. fluorine) or donating (e.g. alkyl or methoxy) substituents has the effect of shifting potentials to a more positive or negative value, respectively. This analysis indicates that xanthylium and triphenylmethyl derivates **5**, **3c**, **3e** and **3f** exhibit potentials that are too positive for efficient redox mediation.

Calculated $\Delta G^0_2$ values were used to probe the likelihood of the inner-sphere or outer-sphere mechanism (Table S6, SI). Compounds **1a**, **2a**, **2c**, **3a**, **3b** and **3d** are expected to react spontaneously with oxygen, while $\Delta G^0_2$ values are positive for **1b**, **1c**, **1d**, **1e**, **2b** and **4**. This reactivity trend can be reasoned based on steric effects: the radicals which do not spontaneously react with oxygen each feature a substituted phenyl ring at the C9 position, which imparts significant steric bulk and restricts access to the tertiary carbon-centered radical. The compounds with positive $\Delta G^0_2$ values were viewed as promising candidates for outer-sphere redox mediation and further evaluated with cyclic voltammetry. Step 3 of our computational process was used to evaluate the spontaneity of reaction between organic peroxides formed via the inner-sphere mechanism with $Li^+$-cations. Spontaneity is determined from the sign of $\Delta G^0_3$ values, but we have allowed for 0.5 eV of computational error. In general, $\Delta G^0_3$ values reflect the stability of RO-OR (sterically hindered **2c** makes unstable RO-OR) and $R^+$ (electron-donating o-methoxy and amine groups on **3b** and **3d** decrease the Lewis acidity of these cations, making replacement by $Li^+$ spontaneous). Compounds **1a**, **2a** and **3a** form stable peroxides and were removed as candidates for the inner-sphere redox mediation. However, on account of their mild $\Delta G^0_3$ values, peroxides of **2c**, **3b** and **3d** were selected as potential inner-sphere redox mediators.

To exemplify how calculated thermodynamic parameters affect redox mediation mechanisms, an energy diagram in Figure 2b illustrates three organic cations that are expected either to perform redox mediation, via the inner- and outer-sphere mechanisms (compounds **1c** and **2c**, respectively), or to be catalytically inactive (compound **2a**). The diagram is presented at an applied potential of 3.0 V vs. $Li^+/Li$, to directly illustrate the anticipated overpotentials for each process. All three mediators exhibit positive or mild negative $\Delta G^0_1$ values, which are directly

related to the catalyst overpotential. The positive $\Delta G^0_2$ for **1c** indicates that this cation is not likely to form the organic peroxide RO-OR and is expected to react through the outer-sphere redox mediation mechanism. In contrast, the negative $\Delta G^0_2$ values of **2a** and **2c** suggest that they can react spontaneously with $O_2$ by the inner-sphere reaction. $\Delta G^0_3$ values differentiate **2a** and **2c** as representatives of the non-catalytic and inner-sphere pathways, respectively. Step 3 is highly endergonic for **2a**, indicating that the organic radical RO-OR is too stable and is not likely to react with Li-ions to form $Li_2O_2$. Thus, **2a** is expected to be non-catalytic. On the other hand, Step 3 is only mildly endergonic for **2c**, suggesting that it may reasonably function as an inner-sphere redox mediator. Based on these screening criteria, cations **1b, 1c, 1d, 1e, 2b, 2c, 3b, 3d** and **4** are viewed as promising candidates for discharge redox mediation in Li-$O_2$ batteries via either the inner- or outer-sphere mechanism (Table S6, SI).

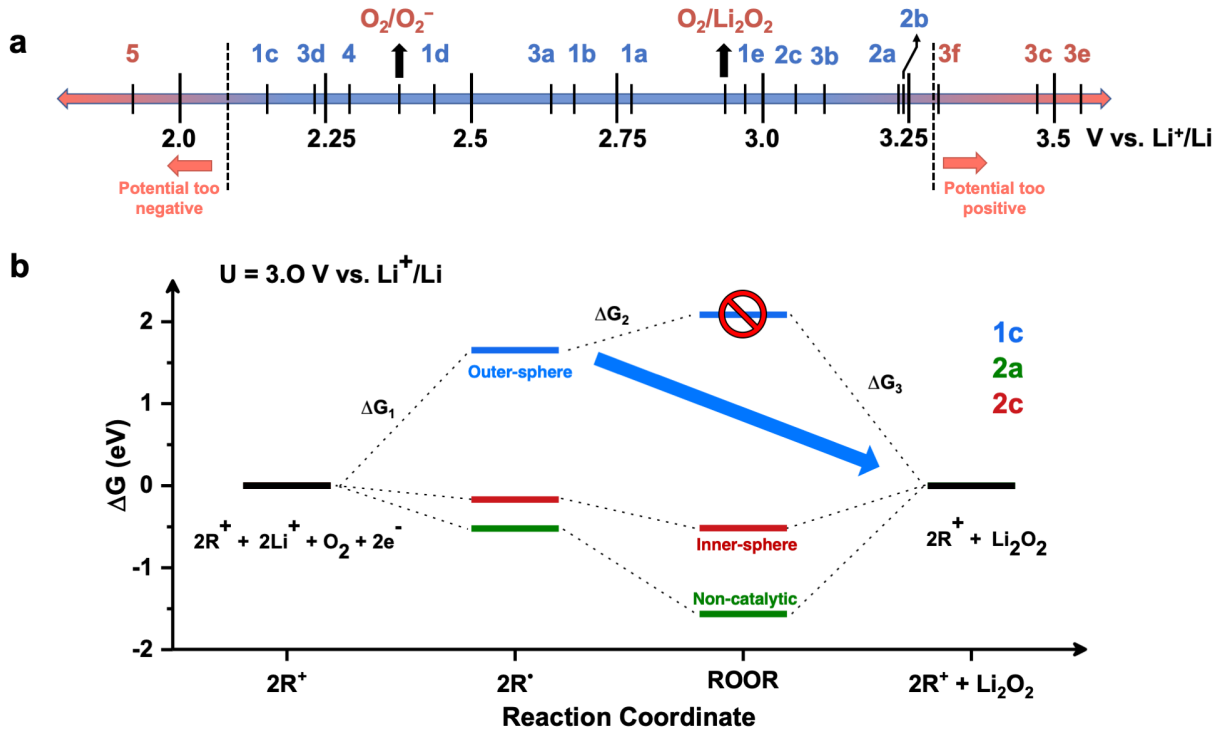


**Figure 2.** Computational screening of redox mediators: a) DFT-computed $R^+/R^\bullet$ standard reduction potentials for each redox mediator candidate, along with the potential for $O_2/O_2^-$ reduction in acetonitrile (ACN) and thermodynamic potential for the overall $O_2/Li_2O_2$ reaction[70]. Redox mediator candidates listed in blue have desirable reduction potentials and are within the 2.10 – 3.26 V vs. $Li^+/Li$ window. b) Energy diagram for selected redox mediators that are predicted to exhibit different behavior: **1c** ($\Delta G^0_2$ is uphill, outer-sphere redox mediation), **2c** ($\Delta G^0_3$ is mildly uphill, inner-sphere catalysis and **2a** ($\Delta G^0_3$ is highly uphill, non-catalytic).

**Cyclic Voltammetry (CV)**. Initial experimental investigation of catalyst candidates was performed using CV measurements in $Li^+$-containing Ar- and $O_2$-saturated ACN solutions (Figure 3 shows the selected voltammograms, while the remaining data is presented in Figure S1, Section S1 SI). In the absence of $O_2$, all $R^+$ cations are characterized by a single chemically reversible $R^+/R^\bullet$ reduction and are plotted in the order of decreasing potentials. Generally, the measured $R^+/R^\bullet$ reduction potentials are within +/- 0.3 V of the DFT-calculated values (Table S6,

SI) and their trends can be readily rationalized using electronic effects described in the previous section. Several different behaviors were observed in the presence of $O_2$. In one case, the $R^+/R^\bullet$ peaks were largely unaffected by $O_2$ (**1e** and **2c**), signaling that there is no follow-up reaction between $R^\bullet$ and $O_2$ on our CV timescales. This lack of reactivity is likely associated with the relatively positive reduction potentials of **1e** and **2c**, making $R^\bullet$ insufficiently reducing to enable rapid electron transfer to $O_2$ or the formation of RO-OR. However, it is important to emphasize that this behavior is limited to the kinetic window of our CV measurements and that the DFT-predicted inner- or outer-sphere behavior of **2c** and **1e**, respectively, may be operational on longer timescales.

In the case of **2a** and **2b**, the cathodic $R^+/R^\bullet$ feature shifts to a more positive potential, while the anodic peak disappears in the presence of $O_2$. This behavior is consistent with the EC type mechanism, wherein $R^+/R^\bullet$ reduction is followed by reaction with $O_2$ to form RO-OR through the inner-sphere pathway. The formation of RO-OR was confirmed by the presence of an irreversible oxidation feature observed during the anodic scan, which corresponds to the oxidation of RO-OR (Figure S2)[58]. However, the lack of catalytic current enhancement of $R^+/R^\bullet$ reduction suggested that **2a** and **2b** terminally formed RO-OR and no follow-up reaction with $Li^+$-cations occurred on our CV timescales. To evaluate whether the reaction with $Li^+$ ions occurs on longer timescales, we monitored the reaction between chemically synthesized RO-OR derivatives of **1a** and **2b** and $Li^+$ cations using UV/Vis absorption spectroscopy (Figure S2). Since no observable change occurred after four hours of monitoring, we conclude that **2a** and **2b** are non-catalytic. While these experimental results are consistent with DFT calculated values for **2a**, the formation of peroxide in the case of **2b** was not predicted by DFT ($\Delta G^0_2$ =0.2 eV, Table S6). Although **2a** and **2b** did not show any inner-sphere catalysis, it remains plausible that other redox mediator derivatives, which form less chemically stable peroxides will exhibit spontaneous reactivity with $Li^+$ and thus perform inner-sphere catalysis.

Compounds with the highest degree of catalytic enhancement came from the family of acridinium-based redox mediators shown on the right side of Figure 3 (1b, 1c, 1d and 4). Their behaviors are characterized by taking 1c as an example: in the presence of $O_2$ the $R^+/R^\bullet$ reduction feature shifts to more positive potentials, becomes chemically irreversible and experiences a marked current enhancement. Coupled with our DFT calculations (Table S6), the experimental CV data is indicative of redox mediation by the outer-sphere mechanism. To estimate the rate constants associated with redox mediation, experimental data were simulated using the following chemical steps (see Section S1 for more info):

$$R^+ + e^- \rightleftarrows R^\cdot \qquad k_1 \quad (1)$$

$$R^\cdot + O_2 \rightleftarrows R^+ + O_2^- \qquad K_{eq,2},\ k_2,\ k_{-2} \quad (2)$$

Fitted $k_1$ values ranged from 0.013-0.020 cm/s, confirming that fast electron transfer between the electrode and redox mediators takes place[72,73]. The resulting rate constants ($k_2$) are plotted with respect to redox mediator standard reduction potential ($E_{R+/R\bullet}$) in Figure 5a. Noticeably, the level of catalytic enhancement increases as $E_{R+/R\bullet}$ becomes more negative (Figure 3). This trend is consistent with the analysis reported by Savéant, who predicted three possible regions

for log($k_2$) vs $E_{R+/R\bullet}$ data, depending on whether the reaction is under control by molecular diffusion or by the electron transfer step (activation control)[74,75]. Our data exhibit dependence that is consistent with activation control, so the data in Figure 5a was fit to the following expression:

$$\log(k_2) = \log(k_s) - \frac{\alpha}{0.058}(E_{\mathrm{R+/R\bullet}} - E_{O2/O2-}) \quad (3)$$

Where $k_s$ is the solution electron exchange rate constant, α is taken to be 0.5 and $E_{O2/O2-}$ is 2.40 V vs. $Li^+/Li$. The fit to our experimental data provided a $k_s$ value of $1.096 \cdot 10^7\ M^{-1}\,s^{-1}$, which agrees well with other studies on outer-sphere redox mediators[74–76].

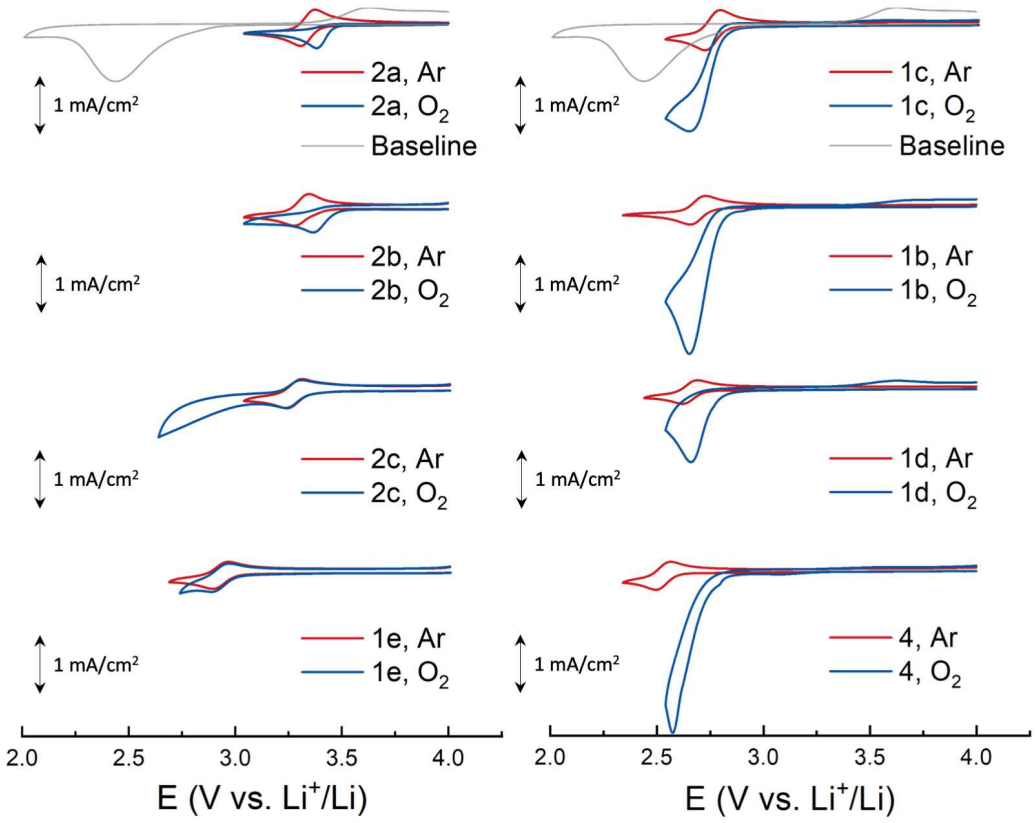


**Figure 3.** Cyclic voltammograms of redox mediators showing their effect on oxygen reduction in Li-$O_2$ cells. CVs of redox mediators in Ar- (red trace) and $O_2$-saturated (blue trace) electrolyte and redox mediator-free solutions (grey) are shown. CVs were recorded in ACN containing 0.1 M tetrabutylammonium perchlorate (TBAP), 10 mM lithium triflate (LiOTF), and 1 mM redox mediator at the scan rate of 100 mV/s.

Two key conclusions can be drawn from our CV analysis. First, the inner-sphere mechanism involving peroxide formation does not result in catalytic ORR. While some radicals, $R^\bullet$, exhibit spontaneous reactivity with $O_2$, the corresponding peroxides are inert toward $Li^+$ ions,

preventing the closure of the catalytic cycle. Even though none of our $R^+$ derivatives showed an inner-sphere catalytic mechanism, it is possible that a such process can be achieved in other derivatives whose energetics are tuned to satisfy the energy landscape illustrated in Figure 2b. Second, cations with standard $R^+/R^\bullet$ potentials in the 2.5-2.77 V vs $Li/Li^+$ range show detectable catalytic enhancements via the outer-sphere mechanism. The catalytic rate constant increases with the thermodynamic driving force for electron transfer from $R^\bullet$ to $O_2$, as predicted by the normal region of the Marcus electron transfer model[74–76]. Cations with $E_{R+/R\bullet}$ potentials more positive than 2.77 V vs $Li/Li^+$ did not show catalytic enhancements, likely because the timescale of the CV experiment was too fast to enable the detectable catalytic enhancement of slower electron transfer processes.

**Battery Discharge**

The influence of outer-sphere redox mediation on Li-$O_2$ cell discharge was evaluated in Li-$O_2$ Swagelok cells, as described in the Methods section. In the absence of redox mediators (Figure 4, gray trace), the cell potential quickly reaches the 2.0 V cutoff potential after a discharge capacity of 0.05 mAh $cm^{-2}$. This rapid cell termination is attributed to the surface-mediated reduction of $O_2$ and passivation of the gas diffusion layer (GDL) by a $Li_2O_2$ film[3]. In the presence of redox mediators, discharge capacity increased, which is consistent with the redox mediation observed in CVs. In general, discharge capacities were found to increase with the concentration of a redox mediator (Figure S7). This behavior is likely due to the presence of two competing pathways for $Li_2O_2$ formation: (i) un-catalyzed $Li_2O_2$ formation that results in $Li_2O_2$ films on the electrode surface and its passivation and (ii) desired redox mediation which moves the site for $Li_2O_2$ formation and growth away from the electrode and into the solution phase. At higher $R^+$ concentrations, the redox mediated process is more dominant, resulting in larger discharge capacities. Given these experimental results, the performance of each mediator was evaluated at its solubility limit (Figure 4a). The $Li_2O_2$ formation was confirmed using Raman spectroscopy (Figure S8), scanning electron microscopy (SEM) imaging (Figure S9) and UV-Vis titration with a $TiOSO_4$ reagent (Table S5). Discharge plateaus of redox mediator-containing cells appear at lower overpotentials and tend to scale with $E_{R+/R\bullet}$. The discharge capacities of redox mediator-containing cells achieved significantly larger capacities before reaching the 2.0 V termination potential. The overall capacity enhancements ranged from 8- to 26-fold and are attributed to redox mediation moving the $O_2/O_2^-$ reduction into solution and mitigating the surface-mediated route. The best performance was observed with 1b, providing capacities that are competitive with those reported for quinone-based and other mediators[6–22] (for comparison, a best-performing quinone-based redox mediator, DBBQ[18], is shown in Figure 4a). Overall, these results are encouraging and provide evidence that the organic cations in Scheme 1 provide an important expansion of the library of functional redox-mediators for Li-$O_2$ batteries.

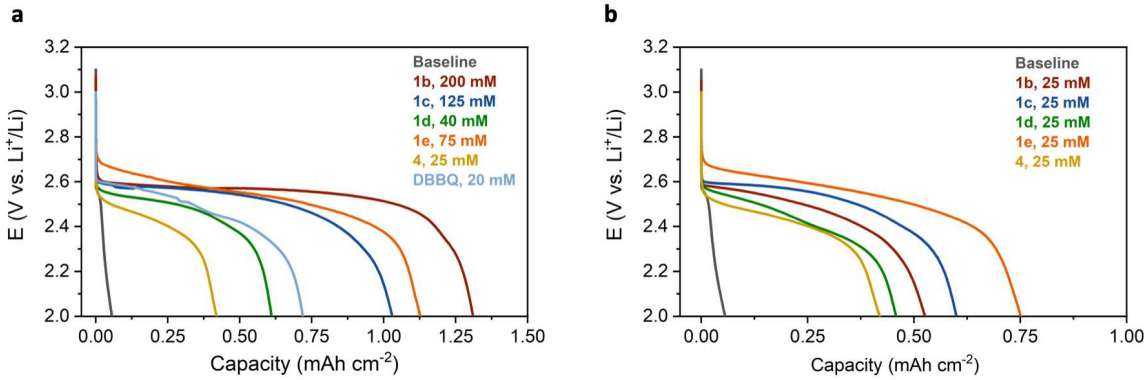


**Figure 4.** a) Battery discharge curves for Li-$O_2$ cells prepared with 1 M LiOTF in TEGDME and redox mediators at maximum concentrations (1b, 200 mM; 1c, 125 mM; 1d, 40 mM; 1e, 75 mM; 4, 25 mM; DBBQ, 20 mM). b) Battery discharge curves for Li-$O_2$ cells prepared with uniform 25 mM redox mediator concentrations. Both panels show the discharge curve from a redox mediator-free, baseline cell (black trace).

To obtain a more quantitative comparison, redox mediators were tested at a uniform concentration of 25 mM (Figure 4b). Surprisingly, battery discharge capacity was found to increase with more positive values of $E_{R+/R\bullet}$, which is counterintuitive based on the observed relationship between $E_{R+/R\bullet}$ and log($k_2$) in the CV section. Equation 3 predicts that the rate of redox mediation will increase as the thermodynamic driving force available to the reaction between $R^\bullet$ and $O_2$ increases, i.e., the more negative $E_{R+/R\bullet}$, as expected for the electron transfer occurring within the normal Marcus region. Here, however, the opposite behavior is observed. To illustrate this, the results from our CV and chronopotentiometry measurements are compared in Figure 5a, by showing how bimolecular rate constants $k_2$ (blue points) and battery discharge capacities (red bars) change as a function of $E_{R+/R\bullet}$. Clearly, the redox mediators that react more slowly with $O_2$ yield larger discharge capacities. Such strikingly opposing trends observed in CV and battery discharge data indicate that relying on CV screening for discovery of novel redox mediators may be ill-advised. CV measurements probe the electrochemical processes that occur on short timescales that vary in the the microseconds-to-seconds range, depending on the sweep rate used in the CV experiment. As such, CV is an excellent tool to study kinetics of electron transfer reactions. On the other hand, the capacity of the battery depends on the chemical processes, such as the growth of $Li_2O_2$ crystals, that take place at timescales that are much longer than the temporal window of the CV technique. The opposing trends observed in Figure 5a clearly point to the dangers associated with relying solely on CV to screen for efficient redox mediators.

The trend observed in Figure 5a can be explained by the competition between un-catalyzed and catalyzed $O_2/Li_2O_2$ reduction processes. The un-catalyzed process is known to result in rapid cell death because of the electrode surface passivation by the electrochemically insulating $Li_2O_2$ films[3]. Since the un-catalyzed process occurs at potentials near 2.53 V vs. $Li^+/Li$, any redox mediator with $E_{R+/R\bullet}$ values near that potential will be inefficient in competing with the un-catalyzed process. Such mediators could be made more competitive if their concentration is

significantly higher than that of $O_2$, and this avenue of research should be explored further. At millimolar redox mediator concentrations used in this study, both $O_2$ and $R^+$ species are available near the electrode surface, leading to the competition between the un-catalyzed and redox mediated processes.

Given the observed increase in the battery discharge capacity with increased $E_{R+/R\bullet}$ values, it is highly probable that further improvements are expected if redox mediators with more positive potentials are utilized. However, the rate of the redox mediated process will become increasingly thermodynamically unfavorable as the $E_{R+/R\bullet}$ of the redox mediator increases, eventually leading to loss of activity. A possible solution to this challenge is to increase the concentration of the redox mediator: at high concentrations of electrochemically generated $R^\bullet$, the electron transfer to $O_2$ will be thermodynamically favorable, even for highly positive $E_{R+/R\bullet}$ values, because of the equilibrium shift caused by Le Chatelier's principle. Thus, a critical question remains: how positive can $E_{R+/R\bullet}$ of a redox mediator be pushed with it still able to mediate $O_2$ reduction? To obtain a more quantitative comparison, the chronopotentiometric response was simulated using a model that involves redox mediated $O_2$ reduction described by equation 4. The solution to the relevant differential equations (Methods section) provides the conditions for redox catalysis:

$$redox\ catalysis = \begin{cases} yes\ if\ F \cdot C_{R+}^0 \cdot \sqrt{D \cdot (k_2 \cdot C_{O2})} \geq i_0 \\ no\ if\ F \cdot C_{R+}^0 \cdot \sqrt{D \cdot (k_2 \cdot C_{O2})} < i_0 \end{cases} \quad (4)$$

where F is Faraday's constant, $C_{R+}^0$ is the concentration of redox mediator, D is the diffusion coefficient of the redox mediator, $k_2$ is the bimolecular rate constant for reaction between $R^\bullet$ and $O_2$ and $C_{O2}$ is the concentration of $O_2$ in the cell which was taken to be the solubility of $O_2$ in TEGDME (0.8 mM)[77]. This equation provides the ranges of current densities ($i_0$), redox mediator concentrations ($C_{R+}^0$) and redox mediator potentials ($E_{R+/R\bullet}$) (expressed in the rate constant $k_2$ via equation 3) which are expected to yield the redox mediated reaction. For example, Figure 5b plots the redox mediated (blue) and non-catalyzed (white) zones for three specified $E_{R+/R\bullet}$ values ($E_{R+/R\bullet}$ =2.7, 3.0 and 3.3 V vs. $Li^+/Li$). To help illustrate the meaning of this plot, a single current density of 1 mA $cm^{-2}$ was chosen and indicated by the horizontal dashed line in Figure 5b. The point where the dashed line intercepts the borders of the three shaded regions, marked as A, B and C, respectively, determines the minimum redox mediator concentration required to achieve redox catalysis for a specified $E_{R+/R\bullet}$. Points A and C illustrate that, as $E_{R+/R\bullet}$ values increase from 2.7 to 3.3 V, increasing concentrations of redox mediator (from 0.7 to 187 mM) are needed to maintain the redox mediation conditions. Clearly, this model uncovers that redox mediation can be achieved for a wide range of $E_{R+/R\bullet}$, as long as the concentration of the redox mediator is increased to the value dictated by equation 4. Under such high concentrations of redox mediator, the process is no longer "catalytic", because a large portion of reduced redox mediator is never converted to its cationic form. Nonetheless, the discharge capacity invested to reduce the redox mediator is very small relative to that involved in the formation of $Li_2O_2$, because the $O_2$ concentration in the electrolyte solution is constantly replenished by new $O_2$ molecules from air, as dictated by Henry's law. This analysis provides

clear guidelines for the discovery of future discharge redox mediators with increased discharge capacities: redox mediators with $E_{R+/R\bullet}$ values of 3.0 V or above should be explored for discharge redox mediation and their solubility in the electrolyte should be higher than 10 mM.

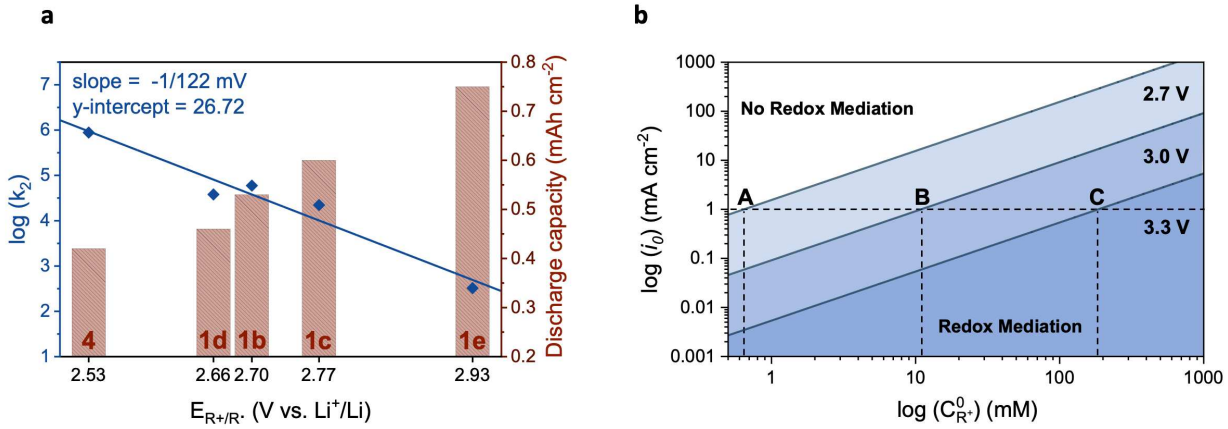


**Figure 5.** a) Plot of rate constants $k_2$ (blue points) and discharge capacities (red histogram) as a function of $E_{R+/R\bullet}$. Discharge capacities were obtained from data in Figure 4b. b) Chronopotentiometry simulations showing catalytic (blue) and noncatalytic (white) regions for a wide range of current densities $i_0$ and redox mediator concentrations. Equation 4 was used to plot the graphs for three different redox mediator potentials: $E_{R+/R\bullet}$ of 2.7, 3.0 and 3.3 V. The points A, B and C correspond to the current density $i_0 = 1$ mA cm$^{-2}$ and show the minimum redox mediator concentrations required to achieve redox catalysis for a chosen $E_{R+/R\bullet}$.

**Conclusions**

A new class of triarylmethyl cation discharge redox mediators for Li-$O_2$ batteries was investigated using a combination of computational and experimental studies. While both inner- and outer-sphere mechanisms were explored computationally, the experimental work shows that only the outer-sphere mechanism results in the closure of the catalytic cycle. The inner-sphere redox mediation candidates led to formation of stable RO-OR intermediates, which did not result in catalytic activity. Furthermore, the increased rate of reaction between redox mediators and oxygen with more negative values of $E_{R+/R\bullet}$ was indicative of activation control of outer-sphere redox mediation and Marcus-type rate dependence on the thermodynamic driving force. Enhancements to Li-$O_2$ discharge capacity rivalling those of well-studied quinone-based mediators were realized, providing a new class of molecular motifs whose derivatives can be explored as future redox mediators. Comparative CV and chronopotentiometric studies have resulted in an interesting finding: improved discharge capacities were obtained for kinetically "sluggish" redox mediators. More specifically, a clear relationship between discharge capacity and more positive $E_{R+/R\bullet}$ values was observed, which underscores the importance of controlling discharge potential to improve capacity. The observed behavior is explained by a competition between uncatalyzed and redox mediated oxygen reduction, with the uncatalyzed process being less efficient as the cell potential becomes more positive. To evaluate the zones of current densities, redox mediator potentials and concentrations in which redox mediation is possible,

chronopotentiometry simulations were performed. These simulations predicted that redox mediation can be achieved for $E_{R+/R\bullet}$ values as positive as 2.96 V, but that they must be operated at high concentrations to enable spontaneous electron transfer to $O_2$ using Le Chatelier's principle. Based on the desire to reduce the discharge overpotential and prolong battery discharge times, this finding will be instrumental for the discovery of future redox mediators with more positive reduction potentials that may be prepared at high concentrations.


1. Kwak, W.-J. *et al.* Lithium–Oxygen Batteries and Related Systems: Potential, Status, and Future. *Chem. Rev.* **120**, 6626–6683 (2020).
2. Aurbach, D., McCloskey, B. D., Nazar, L. F. & Bruce, P. G. Advances in understanding mechanisms underpinning lithium–air batteries. *Nat. Energy* **1**, 16128 (2016).
3. Viswanathan, V. *et al.* Electrical conductivity in $Li_2O_2$ and its role in determining capacity limitations in non-aqueous Li-$O_2$ batteries. *J. Chem. Phys.* **135**, 214704 (2011).
4. Aetukuri, N. B. *et al.* Solvating additives drive solution-mediated electrochemistry and enhance toroid growth in non-aqueous Li–$O_2$ batteries. *Nat. Chem.* **7**, 50–56 (2015).
5. Burke, C. M., Pande, V., Khetan, A., Viswanathan, V. & McCloskey, B. D. Enhancing electrochemical intermediate solvation through electrolyte anion selection to increase nonaqueous Li–$O_2$ battery capacity. *Proc. Natl. Acad. Sci.* **112**, 9293–9298 (2015).
6. Zhang, Y. *et al.* Potential-Dependent Generation of $O_2^-$ and $LiO_2$ and Their Critical Roles in $O_2$ Reduction to $Li_2O_2$ in Aprotic Li–$O_2$ Batteries. *J. Phys. Chem. C* **120**, 3690–3698 (2016).
7. Dai, A., Li, Q., Liu, T., Amine, K. & Lu, J. Fundamental Understanding of Water-Induced Mechanisms in Li–$O_2$ Batteries: Recent Developments and Perspectives. *Adv. Mater.* **31**, 1805602 (2019).
8. Liu, T. *et al.* The Effect of Water on Quinone Redox Mediators in Nonaqueous Li-$O_2$ Batteries. *J. Am. Chem. Soc.* **140**, 1428–1437 (2018).
9. Han, X.-B. & Ye, S. Structural Design of Oxygen Reduction Redox Mediators (ORRMs) Based on Anthraquinone (AQ) for the Li–$O_2$ Battery. *ACS Catal.* **10**, 9790–9803 (2020).
10. Tesio, A. Y. *et al.* Organic radicals for the enhancement of oxygen reduction reaction in Li–$O_2$ batteries. *Chem. Commun.* **51**, 17623–17626 (2015).
11. Blanchard, R., Martin, V., Mantoux, A. & Chatenet, M. Cobalt porphyrin and Salcomine as novel redox shuttle species to enhance the oxygen evolution reaction in Li–$O_2$ batteries. *Electrochim. Acta* **261**, 384–393 (2018).
12. Ko, Y. *et al.* Biological Redox Mediation in Electron Transport Chain of Bacteria for Oxygen Reduction Reaction Catalysts in Lithium–Oxygen Batteries. *Adv. Funct. Mater.* **29**, 1805623 (2019).
13. Lacey, M. J., Frith, J. T. & Owen, J. R. A redox shuttle to facilitate oxygen reduction in the lithium air battery. *Electrochem. Commun.* **26**, 74–76 (2013).
14. Yang, L., Frith, J. T., Garcia-Araez, N. & Owen, J. R. A new method to prevent degradation of lithium–oxygen batteries: reduction of superoxide by viologen. *Chem. Commun.* **51**, 1705–1708 (2015).
15. Hwang, C. *et al.* Biomimetic Superoxide Disproportionation Catalyst for Anti-Aging Lithium–Oxygen Batteries. *ACS Nano* **13**, 9190–9197 (2019).
16. Ren, M. *et al.* Bioinspired Redox Mediator in Lithium–Oxygen Batteries. *ACS Catal.* **11**, 1833–1840 (2021).

17. Zhang, P. *et al.* Promoting Surface-Mediated Oxygen Reduction Reaction of Solid Catalysts in Metal–$O_2$ Batteries by Capturing Superoxide Species. *J. Am. Chem. Soc.* **141**, 6263–6270 (2019).
18. Gao, X., Chen, Y., Johnson, L. & Bruce, P. G. Erratum: Promoting solution phase discharge in Li–$O_2$ batteries containing weakly solvating electrolyte solutions. *Nat. Mater.* **15**, 918 (2016).
19. Matsuda, S., Hashimoto, K. & Nakanishi, S. Efficient $Li_2O_2$ Formation via Aprotic Oxygen Reduction Reaction Mediated by Quinone Derivatives. *J. Phys. Chem. C* **118**, 18397–18400 (2014).
20. Sun, D. *et al.* A Solution-Phase Bifunctional Catalyst for Lithium–Oxygen Batteries. *J. Am. Chem. Soc.* **136**, 8941–8946 (2014).
21. Zhang, Y. *et al.* High-Capacity and High-Rate Discharging of a Coenzyme Q10-Catalyzed Li–$O_2$ Battery. *Adv. Mater.* **30**, 1705571 (2018).
22. Zhang, J. *et al.* A versatile functionalized ionic liquid to boost the solution-mediated performances of lithium-oxygen batteries. *Nat. Commun.* **10**, 602 (2019).
23. Lee, J.-S., Lee, C., Lee, J.-Y., Ryu, J. & Ryu, W.-H. Polyoxometalate as a Nature-Inspired Bifunctional Catalyst for Lithium–Oxygen Batteries. *ACS Catal.* **8**, 7213–7221 (2018).
24. Xiong, Q., Huang, G. & Zhang, X.-B. High-Capacity and Stable Li-$O_2$ Batteries Enabled by a Trifunctional Soluble Redox Mediator. *Angew. Chemie Int. Ed.* **59**, 19311–19319 (2020).
25. Lee, D. *et al.* Direct Observation of Redox Mediator-Assisted Solution-Phase Discharging of Li–$O_2$ Battery by Liquid-Phase Transmission Electron Microscopy. *J. Am. Chem. Soc.* **141**, 8047–8052 (2019).
26. Kwak, W.-J. *et al.* Understanding the behavior of Li–oxygen cells containing LiI. *J. Mater. Chem. A* **3**, 8855–8864 (2015).
27. Kwak, W.-J. *et al.* Li–$O_2$ cells with LiBr as an electrolyte and a redox mediator. *Energy Environ. Sci.* **9**, 2334–2345 (2016).
28. Sharon, D. *et al.* Catalytic Behavior of Lithium Nitrate in Li-$O_2$ Cells. *ACS Appl. Mater. Interfaces* **7**, 16590–16600 (2015).
29. Liu, T. *et al.* Cycling Li-$O_2$ batteries via LiOH formation and decomposition. *Science (80-. ).* **350**, 530–533 (2015).
30. Yu, W. *et al.* A soluble phenolic mediator contributing to enhanced discharge capacity and low charge overpotential for lithium-oxygen batteries. *Electrochem. Commun.* **79**, 68–72 (2017).
31. Rastegar, S. *et al.* High-Rate Long Cycle-Life Li-Air Battery Aided by Bifunctional $InX_3$ (X = I and Br) Redox Mediators. *ACS Appl. Mater. Interfaces* **13**, 4915–4922 (2021).
32. Zhang, C. *et al.* A Comparative Study of Redox Mediators for Improved Performance of Li–Oxygen Batteries. *Adv. Energy Mater.* **10**, 2000201 (2020).
33. Ahmadiparidari, A. *et al.* Enhancing the performance of lithium oxygen batteries through combining redox mediating salts with a lithium protecting salt. *J. Power Sources* **491**, 229506 (2021).
34. Yang, H., Wang, Q., Zhang, R., Trimm, B. D. & Whittingham, M. S. The electrochemical behaviour of TTF in Li–$O_2$ batteries using a TEGDME-based electrolyte. *Chem. Commun.* **52**, 7580–7583 (2016).
35. Bergner, B. J., Schürmann, A., Peppler, K., Garsuch, A. & Janek, J. TEMPO: A Mobile

Catalyst for Rechargeable Li-$O_2$ Batteries. *J. Am. Chem. Soc.* **136**, 15054–15064 (2014).
36. Bergner, B. J. *et al.* Understanding the fundamentals of redox mediators in Li–$O_2$ batteries: a case study on nitroxides. *Phys. Chem. Chem. Phys.* **17**, 31769–31779 (2015).
37. Lim, H.-D. *et al.* Rational design of redox mediators for advanced Li–$O_2$ batteries. *Nat. Energy* **1**, 16066 (2016).
38. Xu, C. *et al.* Bifunctional Redox Mediator Supported by an Anionic Surfactant for Long-Cycle Li–$O_2$ Batteries. *ACS Energy Lett.* **2**, 2659–2666 (2017).
39. Feng, N., He, P. & Zhou, H. Enabling Catalytic Oxidation of $Li_2O_2$ at the Liquid–Solid Interface: The Evolution of an Aprotic Li–$O_2$ Battery. *ChemSusChem* **8**, 600–602 (2015).
40. Kundu, D., Black, R., Adams, B. & Nazar, L. F. A Highly Active Low Voltage Redox Mediator for Enhanced Rechargeability of Lithium–Oxygen Batteries. *ACS Cent. Sci.* **1**, 510–515 (2015).
41. Kwak, W.-J., Kim, H., Jung, H.-G., Aurbach, D. & Sun, Y.-K. Review–A Comparative Evaluation of Redox Mediators for Li-$O_2$ Batteries: A Critical Review. *J. Electrochem. Soc.* **165**, A2274–A2293 (2018).
42. Kwak, W.-J. *et al.* Oxidation Stability of Organic Redox Mediators as Mobile Catalysts in Lithium–Oxygen Batteries. *ACS Energy Lett.* **5**, 2122–2129 (2020).
43. Mahne, N. *et al.* Singlet oxygen generation as a major cause for parasitic reactions during cycling of aprotic lithium–oxygen batteries. *Nat. Energy* **2**, 17036 (2017).
44. Houchins, G., Pande, V. & Viswanathan, V. Mechanism for Singlet Oxygen Production in Li-Ion and Metal–Air Batteries. *ACS Energy Lett.* **5**, 1893–1899 (2020).
45. Kwak, W.-J. *et al.* Deactivation of redox mediators in lithium-oxygen batteries by singlet oxygen. *Nat. Commun.* **10**, 1380 (2019).
46. Gao, X., Chen, Y., Johnson, L. R., Jovanov, Z. P. & Bruce, P. G. A rechargeable lithium–oxygen battery with dual mediators stabilizing the carbon cathode. *Nat. Energy* **2**, 17118 (2017).
47. Weerasooriya, R. B. *et al.* Kinetics of Hydride Transfer from Catalytic Metal-Free Hydride Donors to $CO_2$. *J. Phys. Chem. Lett.* **12**, 2306–2311 (2021).
48. Lim, C.-H. *et al.* Benzimidazoles as Metal-Free and Recyclable Hydrides for $CO_2$ Reduction to Formate. *J. Am. Chem. Soc.* **141**, 272–280 (2019).
49. Walpita, J. *et al.* Pourbaix diagrams in weakly coupled systems: a case study involving acridinol and phenanthridinol pseudobases. *J. Phys. Org. Chem.* **29**, 204–208 (2016).
50. Zoric, M. R., Kadel, U. P. & Glusac, K. D. Cocatalysis: Role of Organic Cations in Oxygen Evolution Reaction on Oxide Electrodes. *ACS Appl. Mater. Interfaces* **10**, 26825–26829 (2018).
51. Ilic, S., Pandey Kadel, U., Basdogan, Y., Keith, J. A. & Glusac, K. D. Thermodynamic hydricities of biomimetic organic hydride donors. *J. Am. Chem. Soc.* **140**, 4569–4579 (2018).
52. Ilic, S., Alherz, A., Musgrave, C. B. & Glusac, K. D. Thermodynamic and kinetic hydricities of metal-free hydrides. *Chem. Soc. Rev.* **47**, 2809–2836 (2018).
53. Yang, X. *et al.* Mechanistic studies of electrode-assisted catalytic oxidation by flavinium and acridinium cations. *ACS Catal.* **4**, 2635–2644 (2014).
54. Zoric, M. R. *et al.* Conformational flexibility of xanthene-based covalently linked dimers. *J. Phys. Org. Chem.* **29**, 505–513 (2016).

55. Zoric, M. R., Singh, V., Zeller, M. & Glusac, K. D. Conformational analysis of diols: Role of the linker on the relative orientation of hydroxyl groups. *J. Phys. Org. Chem.* **32**, e3975 (2019).
56. Mirzakulova, E. *et al.* Electrode-assisted catalytic water oxidation by a flavin derivative. *Nat. Chem.* **4**, 794 (2012).
57. Ilic, S., Alherz, A., Musgrave, C. B. & Glusac, K. D. Importance of proton-coupled electron transfer in cathodic regeneration of organic hydrides. *Chem. Commun.* **55**, 5583–5586 (2019).
58. Hogan, D. T. & Sutherland, T. C. Modern Spin on the Electrochemical Persistence of Heteroatom-Bridged Triphenylmethyl-Type Radicals. *J. Phys. Chem. Lett.* **9**, 2825–2829 (2018).
59. Erabi, T., Asahara, M., Miyamoto, M., Goto, K. & Wada, M. 9-Phenylxanthen-9-ylium and 9-Phenylthioxanthen-9-ylium Ions: Comparison of o- and p-Substitutions in the 9-Phenyl Group by Cyclic Voltammetry and Visible Spectra. *Bull. Chem. Soc. Jpn.* **75**, 1325–1332 (2002).
60. Dolganov, A. V *et al.* Acridinium salts as metal-free electrocatalyst for hydrogen evolution reaction. *Electrochem. Commun.* **68**, 59–61 (2016).
61. Wilger, D. J., Grandjean, J.-M. M., Lammert, T. R. & Nicewicz, D. A. The direct anti-Markovnikov addition of mineral acids to styrenes. *Nat. Chem.* **6**, 720–726 (2014).
62. Romero, N. A., Margrey, K. A., Tay, N. E. & Nicewicz, D. A. Site-selective arene C-H amination via photoredox catalysis. *Science (80-. ).* **349**, 1326–1330 (2015).
63. Ilic, S., Brown, E. S., Xie, Y., Maldonado, S. & Glusac, K. D. Sensitization of p-GaP with Monocationic Dyes: The Effect of Dye Excited-State Lifetime on Hole Injection Efficiencies. *J. Phys. Chem. C* **120**, 3145–3155 (2016).
64. Gomberg, M. The Existence of Free Radicals. *J. Am. Chem. Soc.* **36**, 1144–1170 (1914).
65. Hapiot, P., Moiroux, J. & Saveant, J. M. Electrochemistry of NADH/$NAD^+$ analogs. A detailed mechanistic kinetic and thermodynamic analysis of the 10-methylacridan/10-methylacridinium couple in acetonitrile. *J. Am. Chem. Soc.* **112**, 1337–1343 (1990).
66. Arnett, E. M., Flowers, R. A., Meekhof, A. E. & Miller, L. Energetics of formation for conjugate xanthyl carbenium ions, carbanions, and radicals by hydride, proton, and electron transfer in solution and their reactions to give symmetrical bixanthyls. *J. Am. Chem. Soc.* **115**, 12603–12604 (1993).
67. Gostowski, R. C., Bailey, T., Bonner, S. D., Emrich, E. E. & Steelman, S. L. Steric hindrance effects on bimolecular coupling rate constants of carbon-centered radicals. *J. Phys. Org. Chem.* **13**, 735–739 (2000).
68. Shi, C. & Anson, F. C. The effect of triphenylmethyl cations on the electroreduction of $O_2$ in nitrobenzene or acetonitrile. *J. Electroanal. Chem.* **484**, 144–149 (2000).
69. Chase, M. W. NIST-JANAF Thermochemical Tables. *J. Phys. Chem. Ref. Data* **9**, 1510 (1998).
70. Vasudevan, D. & Wendt, H. Electroreduction of oxygen in aprotic media. *J. Electroanal. Chem.* **392**, 69–74 (1995).
71. Yang, X. *et al.* Toward Organic Photohydrides: Excited-State Behavior of 10-Methyl-9-phenyl-9,10-dihydroacridine. *J. Phys. Chem. B* **117**, 15290–15296 (2013).
72. Evans, D. H., O'Connell, K. M., Petersen, R. A. & Kelly, M. J. Cyclic voltammetry. *J. Chem.*

*Educ.* **60**, 290 (1983).
73. Brown, J. H. Development and Use of a Cyclic Voltammetry Simulator To Introduce Undergraduate Students to Electrochemical Simulations. *J. Chem. Educ.* **92**, 1490–1496 (2015).
74. Andrieux, C. P., Dumas-Bouchiat, J. M. & Saveant, J. M. Homogeneous redox catalysis of electrochemical reactions: Part II. Rate determining electron transfer, evaluation of rate and equilibrium parameters. *J. Electroanal. Chem. Interfacial Electrochem.* **87**, 55–65 (1978).
75. Andrieux, C. P., Blocman, C., Dumas-Bouchiat, J. M. & Saveant, J. M. Heterogeneous and homogeneous electron transfers to aromatic halides. An electrochemical redox catalysis study in the halobenzene and halopyridine series. *J. Am. Chem. Soc.* **101**, 3431–3441 (1979).
76. Andrieux, C. P., Dumas-Bouchiat, J. M. & Saveant, J. M. Homogeneous redox catalysis of electrochemical reactions: Part I. Introduction. *J. Electroanal. Chem. Interfacial Electrochem.* **87**, 39–53 (1978).
77. Gittleson, F. S., Jones, R. E., Ward, D. K. & Foster, M. E. Oxygen solubility and transport in Li–air battery electrolytes: establishing criteria and strategies for electrolyte design. *Energy Environ. Sci.* **10**, 1167–1179 (2017).

**Methods**

**Synthesis**

Unless otherwise specified, reagents were procured from commercial sources and used as received. $^{1}$H NMR spectra were collected using a Bruker DPX operating at 9.4 T (400 MHz) or Bruker Avance III HD operating at 11.74 T (500 MHz) spectrometers. 2,7-Dimethyl-9-mesityl-10-methylacridinium tetrafluoroborate (**1b**) and 9-mesityl-10-methylacridinium tetrafluoroborate (**1c**) were purchased from Millipore-Sigma and 2,7-difluoro-9-mesityl-10-methylacridinium tetrafluoroborate (**1e**) from AmBeed. [10-Methyl-9-phenylacridinium triflate (**1a**),[58] 9-(2,6-Dimethoxyphenyl)-1,8-dimethoxy-10-methyl-9,10-dihydroacridin-9-ylium perchlorate (**1d**),[63] 9-phenylxanthenium triflate (**2a**),[58] (2-methoxyphenyl) (**3b**),[78] 1,13-dimethoxy-5,9-dimethyl-5,9-dihydro-13-bH-quinolino[2,3,4-kl]acridin-13b-ylium perchlorate (**4**)[63] and tris(2,6-dimethoxyphenyl)methylium perchlorate (**5**),[51] were prepared in our lab according to published literature procedures. The peroxides of **2a** (**2a**/**RO-OR**) and **2b** (**2b**/**RO-OR**) were prepared according to published procedures[59] and their putative structures are reported in Section 1 of the SI.

9-mesityl xanthylium **(2b)** was synthesized by a modified procedure from the literature.[59] Firstly, the xanthenol analog, 9-mesityl-9*H*-xanthen-9-ol, was made, as follows: 1,3,5-trimethylbenzene (72 mg, 0.6 mmol) was dissolved in 1.3 mL dry THF and the solution was purged with Ar. Then, n-BuLi (0.6 mmol, 0.24 mL, 2.5 M) was added to the mixture dropwise at -78°C. The resultant mixture was warmed to room temperature and stirred under Ar for 2 h. The mixture was cooled to 0°C and xanthone (0.1167 g, 0.6 mmol) dissolved in a minimal amount of toluene was added to the solution. The mixture was stirred for 24 h and allowed to warm up to room temperature during that time. The reaction was quenched with water and the product was extracted with dichloromethane. Combined $CH_2Cl_2$ layers were added and dried over anhydrous $MgSO_4$. The solvent was evaporated and yielded a white solid product. $^{1}$H NMR of 9-mesityl-9*H*-xanthen-9-ol matched the already published spectrum.[59]

To make **2b**, a 15-mL vial was charged with 9-mesityl-9*H*-xanthen-9-ol (0.50 mmol) and concentrated perchloric acid (70%, 4 mL). The resulting mixture was stirred overnight. The precipitate that formed was

filtered off, washed with anhydrous ethyl ether (15 mL), and dried in vacuum to give solid product. $^1$H NMR matched what has been previously published.[59]

9-(2,4,6-trimethoxyphenyl)xanthylium **(2c)** was synthesized by a modified procedure from the literature.[59] Firstly, the xanthenol analog, 9-(2,4,6-trimethoxy)-9*H*-xanthen-9-ol, was made, as follows: 1,3,5-trimethoxybenzene (100 mg, 0.6 mmol) was dissolved in 1.3 mL dry THF and the solution was purged with Ar. Then, n-BuLi (0.6 mmol, 0.24 mL, 2.5 M) was added to the reaction mixture dropwise via canula at -78°C. The reaction mixture was allowed to warm to room temperature and stirred under Ar for 2 h. The mixture was cooled to 0°C and xanthone (0.1167 g, 0.6 mmol) dissolved in a minimal amount of toluene was added to the solution. The mixture was stirred for 24 h and allowed to warm up to room temperature during that time. The reaction was quenched with water followed by extraction with $CH_2Cl_2$. Organic layers were merged and dried over anhydrous magnesium sulfate. After $CH_2Cl_2$ was evaporated, it yielded a white solid. $^1$H NMR of 9-(2,4,6-trimethoxy)-9*H*-xanthen-9-ol matched the already published spectrum.[59]

To make the **2c**, a 15-mL vial was charged with 9-(2,4,6-trimethoxy)-9*H*-xanthen-9-ol (0.50 mmol) and concentrated perchloric acid (70%, 4 mL). The resulting mixture was stirred overnight. The precipitate that formed was filtered off, washed with anhydrous ethyl ether (15 mL), and dried in vacuum to give solid product. $^1$H NMR matched what has been previously published.[59]

**Electrochemistry**

Tetrabutylammonium perchlorate was recrystallized from methanol. Lithium triflate was dried under vacuum at 80 °C for three days prior to use. Tetraethylene glycol dimethyl ether (TEGDME) was purchased from Millipore-Sigma and dried over 3 Å activated molecular sieves prior to use. The final water content of TEGDME was < 100 ppm as measured by Karl Fischer titration. CV measurements were performed with a standard three-electrode set up with glassy carbon (GC), 10 mM $Ag/AgNO_3$ and Pt wire serving as the working, reference and counter electrodes, respectively. A Gamry 1010B potentiostat was used for CV measurements.

**Cyclic voltammetry**

All cyclic voltammetry measurements were performed in a three-electrode cell setup using glassy carbon (GC, MF-2012, Bioanalytical systems, 0.075 $cm^2$ surface area), 10 mM $Ag/AgNO_3$ non-aqueous reference electrode (MF-2062, Bioanalytical systems) and Pt wire counter electrode (MW-4130 or MW-1033, Bioanalytical systems) and a Gamry 1010B potentiostat. Working electrodes were polished prior to each individual CV using alumina (CF-1050, Bioanalytical systems) and diamond (MF-2054, Bioanalytical systems) slurry polishes. CV experiments were conducted in dry acetonitrile containing 0.1 M, 10 mM and 1 mM tetrabutyl ammonium perchlorate (TBAP), lithium triflate (LiOTF) and redox mediator, respectively. For $O_2$-free and $O_2$-saturated measurements, solutions were purged for 20 minutes with Ar or $O_2$ gas, respectively. [$O_2$] in CV solutions was measured using a Neo-FoxGT $O_2$ sensor provided by Ocean Insight. All potentials are referenced vs. $Li^+/Li$.

**Battery testing**

Swagelok Li-$O_2$ cells were assembled in an Ar-filled (MBraun) glovebox with $H_2O$ and $O_2$ levels below 0.1 and 3 ppm, respectively, similar to prior descriptions.[18] Carbon GDLs were Freudenberg H23C2 and provided by the Fuel Cell Store. For moisture removal, GDLs were dried under vacuum at 150°C for three days prior to storage in the glovebox. During assembly, a Li metal anode was separated from a single, 5.6 mm diameter GDL disk by a Whatman glass fiber paper separator. Redox mediator-containing, 1M LiOTF TEGDME electrolyte (~0.150 mL) was added to the cathode side and a stainless-steel mesh current

collector was used to cover the GDL. The assembled cells were put inside hermetically sealed glass tubes, purged with dry $O_2$ and discharged on a Maccor battery cycler.

After discharge, Swagelok Li-$O_2$ cells were disassembled to recover the carbon GDL. GDLs were washed with a small amount of dimethoxyethane (DME) and dried on a hot plate in the glovebox. After drying, GDLs, deposits and films were characterized by SEM and Raman.

**$Li_2O_2$ quantification**

$Li_2O_2$ quantification was performed using a previously reported UV-Vis method.[18,79] In brief, the Li-$O_2$ cell was deconstructed and glass fiber separator and GDL were added to a small vial with 5 mL of $TiOSO_4$ in aqueous $H_2SO_4$. $Li_2O_2$ is known to spontaneously react with water to form $H_2O_2$ and in the presence of $TiOSO_4$ a yellowish $[Ti(O_2)]^{2+}$ complex is formed with absorption at 410 nm. A small quantity of each solution was 10-fold diluted to generate appropriate UV-Vis solutions which were compared with a calibration curve made from commercial $Li_2O_2$ (Aldrich).

**Raman spectroscopy**

Raman spectroscopy of GDLs and their discharge products was performed with a Renishaw inVia Reflex Microscope using either 633 (red) or 532 (green) laser light at the Electron Microscopy Core (EMC) at UIC's Research Resources Center (RRC). Inside the glovebox, GDLs were loaded into an air-sensitive Raman cell with a thin quartz glass window for observation.

**SEM imaging**

SEM characterization was carried out using a JEOL JSM-IT500HR SEM in field emission mode which is part of the Electron Microscopy Core (EMC) at the UIC Research Resources Center (RRC). Cleaned and dried GDLs were removed from the Ar glovebox in tightly sealed vials and transferred as quickly as possible to SEM vacuum chamber to minimize air exposure. All images were taken at 6000 X magnification using a 5 keV acceleration voltage.

**DFT calculations**

All calculations were performed on Gaussian 09 or 16[80] software using the computational resources from the Laboratory Computing Resource Center at Argonne National Laboratory. Gas-phase optimization was performed using the B3LYP or uB3LYP hybrid functional[81,82] and 6-311g(d)[83] basis set. Single-point energies were calculated at the same level of theory using diethyl ether solvation as implemented in the IEFPCM model.[84] Vibrational frequency analysis showed the presence of no imaginary frequencies in our optimized structures. Detailed information on evaluation of each step in the catalytic mechanism can be found in Section 2 of the SI.

**Chronopotentiometry Modeling**

Chronopotentiometry simulations were performed using the model involving electron transfer and a follow-up chemical step, as defined by equations 1 and 2 which has been defined previously[85]. Full details on the modeling can be found in Section 3 of the SI.


78. Bah, J., Naidu, V. R., Teske, J. & Franzén, J. Carbocations as Lewis Acid Catalysts: Reactivity and Scope. *Adv. Synth. Catal.* **357**, 148–158 (2015).
79. Hartmann, P. *et al.* A comprehensive study on the cell chemistry of the sodium superoxide ($NaO_2$) battery. *Phys. Chem. Chem. Phys.* **15**, 11661–11672 (2013).
80. Frisch, M. J., Trucks, G. W., Schlegel, H. B., Scuseria, G. E. & Robb, M. A. Gaussian 09,

Revision A.02. (2016).
81. Becke, A. D. Density-functional exchange-energy approximation with correct asymptotic behavior. *Phys. Rev. A* **38**, 3098–3100 (1988).
82. Lee, C., Yang, W. & Parr, R. G. Development of the Colle-Salvetti correlation-energy formula into a functional of the electron density. *Phys. Rev. B* **37**, 785–789 (1988).
83. McLean, A. D. & Chandler, G. S. Contracted Gaussian basis sets for molecular calculations. I. Second row atoms, Z=11–18. *J. Chem. Phys.* **72**, 5639–5648 (1980).
84. Tomasi, J. & Persico, M. Molecular Interactions in Solution: An Overview of Methods Based on Continuous Distributions of the Solvent. *Chem. Rev.* **94**, 2027–2094 (1994).
85. Delahay, P., Mattax, C. C. & Berzins, T. Theory of Voltammetry at Constant Current. IV. Electron Transfer Followed by Chemical Reaction. *J. Am. Chem. Soc.* **76**, 5319–5324 (1954).

**Acknowledgements**
This work was supported by the National Science Foundation (Grant NSF 1954298). The work at Argonne was supported by the U.S. Department of Energy under Contract DE-AC02-06CH11357 from the Vehicle Technologies Office. We gratefully acknowledge the computing resources provided on Bebop, a high-performance computing cluster operated by the Laboratory Computing Resource Center (LCRC) at ANL. We also acknowledge the Electron Microscopy Core (EMC) at UIC's Research Resource's Center (RRC) where a significant amount of post-discharge characterization was performed.

**Author contributions**
E.J.A., M.R.Z., R.A., K.A. and K.D.G. helped with the conception of this manuscript. E.J.A. and M.R.Z. performed the DFT evaluations of redox mediators. E.J.A. performed the CV experiments and analysis. E.J.A. performed the battery discharge experiments and analysis. E.J.A. and R.A. performed the post-discharge product characterization. E.J.A. and K.D.G. analyzed crucial data and wrote the manuscript.

**Competing interests**
The authors declare no competing interests.

**Additional information**
Correspondence and requests for materials should be directed to Ksenija D. Glusac.

# Supplementary Files

This is a list of supplementary files associated with this preprint. Click to download.

- RedoxMediatorSupplementaryInfo.pdf